

THERAPEUTIC EVALUATION OF CHEMICALLY SYNTHESIZED COPPER NANOPARTICLES TO PROMOTE FULL-THICKNESS EXCISIONAL WOUND HEALING

ASHISH KUMAR^a, VINAY PANDIT^b, UPENDRA NAGAICH^{a*}

^aDepartment of Pharmaceutics, Amity Institute of Pharmacy, Amity University, Noida, Uttar Pradesh 201303, India, ^bDepartment of Pharmaceutics, Laureate Institute of Pharmacy, Himachal Pradesh 177101, India
Email: upendra_nagaich@hotmail.com

Received: 26 Jun 2020, Revised and Accepted: 02 Sep 2020

ABSTRACT

Objective: The purpose of this research was, synthesis of copper nanoparticles using environment friendly cementation method and evaluate their wound healing property on full-thickness excisional wound.

Methods: Present study reports the synthesis of CNPs by single-step cementation method. Evaluation of CNPs was endorsed by morphological and chemical properties. Furthermore, CNPs was evaluated for its antibacterial potential and invitro hemocompatibility. Additionally, pharmacological evaluation of CNPs was assessed against excisional wound.

Results: Characterization of final product indicate, particle size of CNPs were ranging from 100-150 nm. CNPs showed significant antibacterial activity (A= 2.1±0.1 mm, B =2.1±0.1 mm, C = 1.9±0.2 mm, at 10µg/ml), along with superior hemocompatibility (RBC cell survival 97±1 %). Further CNPs formulation shows increased level of anti-inflammatory cytokinin's (IL-10, 42.7%) as compared to standard (STD), vehicle control, and normal control groups, attributed to accelerated wound healing (p<0.05 vs STD).

Conclusion: The consequences the present investigation endorse the accelerated wound healing potential of CNPs with its anti-inflammatory potential.

Keywords: Copper nanoparticle, Biocompatibility, Antibacterial potential, Wound healing

© 2020 The Authors. Published by Innovare Academic Sciences Pvt Ltd. This is an open access article under the CC BY license (<http://creativecommons.org/licenses/by/4.0/>)
DOI: <http://dx.doi.org/10.22159/ijap.2020v12i6.38869>. Journal homepage: <https://innovareacademics.in/journals/index.php/ijap>

INTRODUCTION

Wound healing is a complex biological progression; wounding leads to tissue inflammation and the release of several pro-inflammatory cytokines including interferon-gamma (IFN-γ), interleukin [1] (IL-1), and tumor necrosis factors (TNF). The release of pro-inflammatory cytokines consequently recruits monocytes and macrophages [2]. Moreover, IFN-γ, TNF-α, and IL-1β lead to tissue apoptosis, because of the triggering of the innate immunity [3]. Wound healing requires a balance of micro-elements, matrix metalloproteinases, antioxidants, and other factors. Thus, over activation of pro-inflammatory cytokines and obstructed instigation of anti-inflammatory mediates delayed the healing rate of the wound [4].

Inhibition of the production of inflammatory cytokines, inflammatory transduction cascades, reduction of oxidative factors, and prevention of the microbial growth at the wound site may delay the healing rate [5]. Copper has an important role in the synthesis and stabilization of various skin proteins [6]. In addition, copper has been used against both gram-positive and gram-negative bacteria, fungi and vira [7]. Copper is traditionally known for its exceptional antibacterial and anti-inflammatory properties [8]. Moreover, copper enhances the rate of wound healing by providing optimum antibacterial and anti-inflammatory properties [9].

There is increase in the resistance to antibiotics and minimal anti-inflammatory activity, limits the wound healing property of currently available agents [10]. Copper may be a promising therapeutic agent, as it has significant antibacterial, anti-inflammatory, and wound healing potential [11]. However, copper deficiency is the common factor for impaired wound healing; copper nanoparticles (CNPs) having a particle size less than 33.8±0.3 nm have shown significant toxicity when compared to a nanoformulation of particle size 103±0.3 nm [12].

MATERIALS AND METHODS

Materials

Copper nitrate was purchased from Central Drug House, New Delhi, India. Iron powder was purchased from Central Drug House, New

Delhi, India. All other chemicals were of analytical grade, microbial culture *escherichia coli* (MTCC No. 1687), *kocuria rhizophila* (MTCC No. 1541) and *staphylococcus aureus* (MTCC No. 737) were obtained from CSIR-Microbial type culture collection and gene bank, Chandigarh, India. Formulation of 30 µg/ml of CNPs was suspended in 2% of Polyvinylpyrrolidone (PVP) solution and applied to wound exposed areas as treatment.

Instrumentation

Surface plasmon resonance was monitored using a UV-Visible spectrophotometer, Perkin Elmer LAMBDA 950 UV/Vis, operated between 800 to 200 nm wavelength ranges at room temperature. Copper ion concentration in the mother solution was determined by Atomic absorption spectroscopy, Perkin Elmer AA Spectrometers, AAnalyst 400. Fourier-transform infrared spectroscopy of the mother solution and nanoparticles was observed using the ALPHA II FTIR Spectrophotometer Bruker, USA. Hydrodynamic and stability of nanoparticles were determined by, Nanobook 90 plus, Brookhaven, USA and Malvern v2.3 Zeta potential analyser, USA. Morphological parameters were evaluated using, Scanning Electron Microscope, Zeiss Evo HD, Jena, Germany, and Transmission Electron Microscope, Morgagni 268D Fei Electron Optics, USA. Elemental analysis was done using EDS Oxford Instruments, UK. Morphology of the biological samples was done using an inverted microscope, Cosmo laboratory equipment, Ambala, India. The absorbance of immunological samples was evaluated using Erba Lisa Scan EM, Transasia Bio-Medicals Ltd. India.

Preparation of copper nanoparticles

CNPs were prepared using a cementation process. An iron plate having a surface area of 1 cm² is placed in a freshly prepared solution of copper nitrate at 70 °C for 120 min. Freshly prepared nanoparticles were centrifuged at 11700 Relative Centrifugal Force (RCF) for 15 min. The supernatant was discarded, and the nanoparticles were resuspended in fresh distilled water by sonification. This process was repeated until a clear supernatant solution was obtained. Finally, 2% PVP was added to freshly prepared nanoparticles suspension to prevent the formation of larger size nanoparticles by agglomeration of nanoparticles.

SPR studies

Surface plasmon resonance (SPR) of the prepared nanoparticles was obtained, to evidence the formation of CNPs. The freshly cleaned iron plate having the surface area of 1 cm² was placed in a freshly prepared solution of copper nitrate 0.001 M in ultrapure Millipore water at 70 °C. The solution was ultrasonicated, to dislodge freshly prepared CNPs. The sample was withdrawn and measured against the solution of 0.001 M copper nitrate solution [13].

AAS studies

Atomic absorption spectroscopy (AAS) helped, in the determination of the amount of CNPs formed at a specific time interval. An iron plate having a surface area of 1 cm² was added to the 10 ppm solution of copper nitrate at 70 °C and ultrasonicated for 5 min. Periodic sampling was done (0, 10, 20, 30, 60 and 120 min) and filtered using a syringe filter (0.1 µm), to remove synthesized CNPs. The amount of copper ions presents in the mother solution was observed, to determine the completion of the reaction [14].

FTIR studies

Fourier-transform infrared spectroscopy (FTIR) technique was used, to observe the emission of vibrational frequency emitted by resonating molecules. The samples were mixed with potassium bromide and pressed with a high-pressure hydraulic press for pallet formation, to obtain FTIR spectra [15].

DLS studies

Dynamic light scattering (DLS) was used to determine the particle size distribution of the prepared CNPs. A freshly prepared sample (5 ml) was resuspended by ultrasonication and particle size distribution was measured [16].

Zeta studies

Zeta Potential was used to determine the surface charge of the formulation. Freshly prepared sample (5 ml) was resuspended by ultrasonication and measured using a zetasizer [17].

SEM studies

Scanning electron microscopy (SEM) was used to evaluate the surface morphology of the prepared nanoparticles. The sample was resuspended in distilled water and ultrasonicated. One drop of CNPs suspension was air-dried on a glass slide (1x1 cm²) and gold-coated [18].

TEM studies

The morphology of the prepared nanoparticle section with particle size was studied by transmission electron microscopy (TEM). Samples were analyzed using carbon-coated TEM mesh grids of 400 mesh [19].

Elemental studies

Energy-dispersive X-ray spectroscopy (EDS) was done by the freshly resuspended sample and was air-dried on a glass slide of 1 cm² area. With the help of SEM, the specific area was selected, and X-ray dispersion of specific regions was observed. X-ray radiation was bombarded on the surface of prepared nanoparticles. The radiation emitted by the CNPs was observed to evaluate the elemental composition [20].

Study of antibacterial property

Kirby-Bauer disk diffusion susceptibility CNPs was done to evaluate the antibacterial property of synthesized nanoparticles. Suspension of prepared nanoparticles was prepared and tested against standard (STD) solution of amoxicillin 10 µg/ml and evaluated against CNPs suspension 10, 120, and 30 µg/ml. Zone of inhibition was noted and compared against STD at the 12th hr of incubation 37 °C in Luria

Hemagglutinin assay

The biocompatibility of CNPs was studied using the Hemagglutinin assay. About one ml of fresh blood was collated from animals and centrifuged at 5488 RCF (4 °C, 10 min). Supernatant was discarded, and the pallet was resuspended in 60 ml of normal saline. One ml

the prepared solution was added (1:1) to STD (Triton X-100) and CNPs sample and incubated at 37 °C for 1 hr. Smear of Normal Saline (normal control; NC), triton X-100 (Positive control; PC) and, CNPs samples were observed under optical microscope [22].

RBC cell viability assay

To evaluate the *in vitro* biocompatibility of synthesized CNPs was evaluated by haemolysis assay. Fresh blood was collated from Albino wistar rats, through the retro orbital puncture. Suspension of CNPs and STD (Triton X-100) were added to an equal amount (100 µl) of uncoagulated blood sample and incubated in a CO₂ incubator (37 °C, 95% RH) for 1hr. The absorbance was taken at 450 nm and the haemolytic rate was calculated as:

$$100 - \{(SA - NCA)/(PCA - NCA) \times 100\}$$

Where SA is sample absorbance, NCA is negative control absorbance, PCA is positive control absorbance [23].

Animal maintenance

Wistar rats of either sex and weight of 230-250g were used for the present study. All animal experiments were approved by the Institutional animal ethics committee (IAEC), Amity University, A-Block, Noida (approval number: CPCSEA/IAEC/AIP/2016/04/13). The animals were first acclimatized in the institutional animal experimental room (temp 20±2 °C, 60±10 Humidity) at normal day and night cycle for 7 d. All animals were maintained on rat chow and water ad libitum.

Creation of full-thickness excision wound

Animals were anesthetized by intraperitoneal administration of ketamine and xylazine (80 and 10 mg/kg respectively). The dorsal area of the rats was shaved and wiped with a 10 % povidone-iodine solution. On the first day of the experiment, aseptically single wound was created using biopsy punch in each rat with a diameter of 15 mm at the interscapular region of the rat dorsal area. Epithelial wounds were covered with a non-woven polyester dressing (3M Dressing Cover Medipore NonWoven Polyester) [24].

Estimation of epithelization period

The wound epithelialization period was determined by measuring the wound contraction using Vernier Caliper. The epithelization period was measured with the help of the wound contraction rate, which is expressed below.

$$\% \text{ wound contraction rate} = \frac{(\text{Initial wound diameter} - \text{Wound diameter at specific day})}{\text{Initial wound diameter}} \times 100$$

Histological evaluation

Three rats from each group were sacrificed on the 5th and 13th day of the experiment. Sections of wounds were used for histological evaluation. The histological sections were evaluated using hematoxylin and eosin staining for measuring re-epithelization, fibroblast accumulation, polymorphonuclear leukocytes, and collagen formation using an inverted light microscope [25].

Estimation of inflammatory cytokines

The wound healing rate depends on the delicate balance between pro-inflammatory (IL-6, TNF-α) and anti-inflammatory (IL-10) cytokinins. The blood samples were collected on the 5th and 13th day and serum were separated, respectively. The concentration of IL-6, TNF-α and IL-10 were evaluated using enzyme-linked immunoassay ELISA, Ray Biotech, USA [26].

Statistical analysis

All the values were expressed in mean±SD. All data of biochemical parameters were statistically analyzed using one-way ANOVA, followed by Tukey post-hoc (SigmaPlot V12, Systat Software Inc. California, USA).

RESULTS

SPR studies

The copper ions (Cu²⁺) present in the solution of copper nitrate gets reduced to elemental copper (Cu⁰). The free-electron

presents on the surface of freshly prepared CNPs showed the resonance peak at 350-400 nm (fig. 1), indicating the presence of CNPs [13].

AAS studies

The reduction of Cu^{2+} ions to Cu^0 confirms the synthesis of CNPs (fig. 1). AAS indicated the decrease in the concentration of Cu^{2+} ions, which have been reduced to Cu^0 by elemental iron. The decrease in the rate of conversion of Cu^{2+} to Cu^0 indicates the completion of the reaction.

FTIR studies

FTIR is an emission spectrum of copper nitrate and CNPs indicate the characteristic frequency band of ferric nitrate complex at 1629 cm^{-1} (fig. 1), which indicates the successful reduction of copper ions

into elemental copper by iron resulting in ferric nitrate as product formation, confirming CNPs synthesis [13].

DLS studies

The graph obtained by DLS indicates the particle size of the formulation in the range of 80 to 150 nm, with a mean effective diameter of 105 nm (fig. 1). The single peak presence showed uniformly sized nanoparticles, indicating good quality of formulation [16].

Zeta studies

The zeta potential of the formulation was found to $33.11 \pm 2\text{ mV}$ (fig. 1), which is above to the minimum required surface charge potential of $\pm 30\text{ mV}$ for the particle size of 100 nm to overcome the gravitational attraction force to prevent sedimentation and glomerular formation, which may increase the size of CNPs [27].

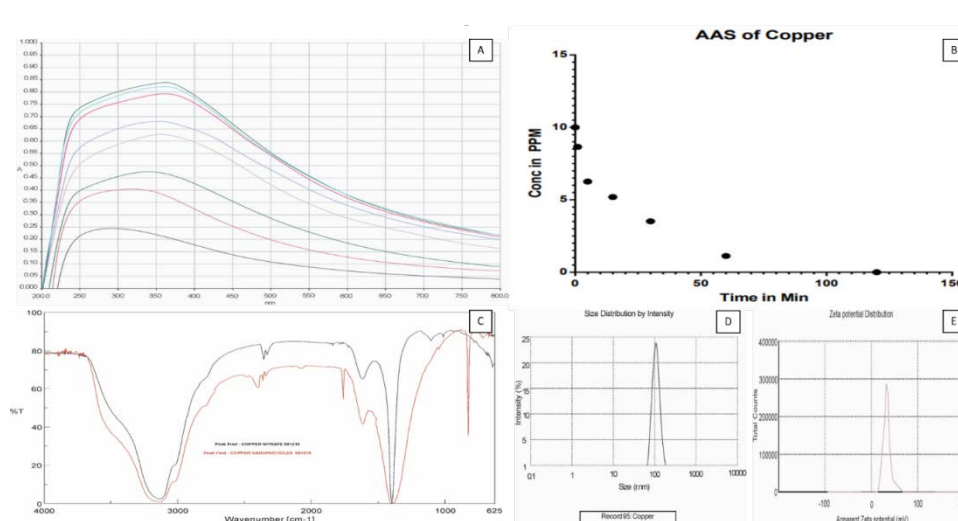


Fig. 1: (A) SPR of CNPs was studied by observing UV-Visible absorption spectra during the synthesis of CNPs. (B) AAS flame spectra of CNPs, show the conversion of ionic copper ions into CNPs. (C) FTIR spectra of copper nitrate and CNPs mother solution, indicating formation of ferric nitrate. (D) DLS spectra of CNPs indicating a hydrodynamic radius of less than 105 ± 2 . (E) Zeta potential of CNPs indicating surface charge $33.11 \pm 2\text{ mV}$

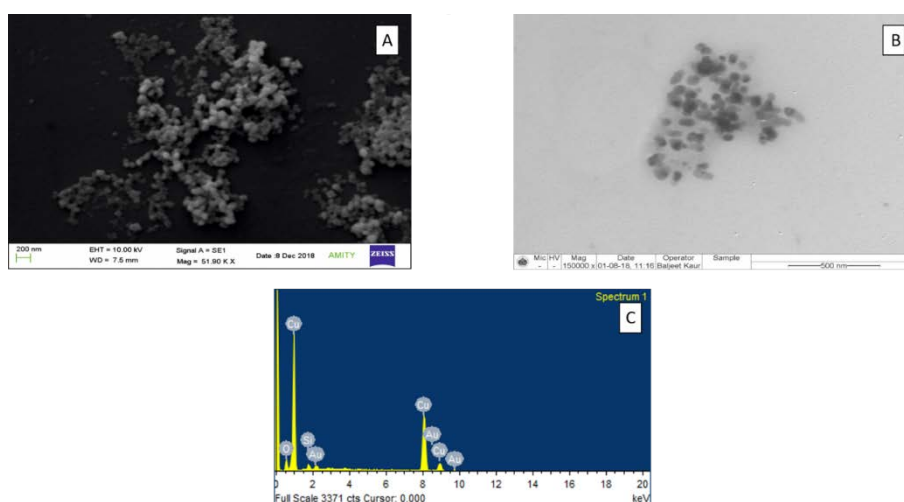


Fig. 2: (A) SEM of CNPs showing particle size of less than 100 nm. (B) TEM of CNPs showing particle size less than 100 nm. (C) EDX of CNPs indicating the presence of copper in CNPs

SEM studies

SEM was done on the electron beam strength of 10.00 kV at 51.90 K X magnification (fig. 2). The morphological evaluation (fig. 2) showed the spherical (uniformly created) nanoparticles having a particle size of less than 100 nm.

TEM studies

TEM scanning of the sample was done with 150 K X magnification. The particle size of the prepared nanoparticles was found to be less than 100 nm (fig. 2), ensuring the non-toxicity of CNPs.

Elemental studies

EDX spectroscopy confirms the presence of the high amount of copper and trace amount of oxygen, indicating very little oxidation of the outer layer of CNPs (fig. 2). The rest of the peak indicates the presence of other elements like Gold and silicon, which may be due to the gold coating of samples for electron microscopy and the base plate is made of silicon glass [20].

Study of antibacterial property

The samples were evaluated using Kirby-Bauer disk diffusion methods. Disk loaded with the CNPs and STD formulation was placed on the culture medium of different microorganisms, the zone of inhibition of CNPs formulation was compared against STD formulation, indicating significant antibacterial activity (fig. 3 A, B, and C).

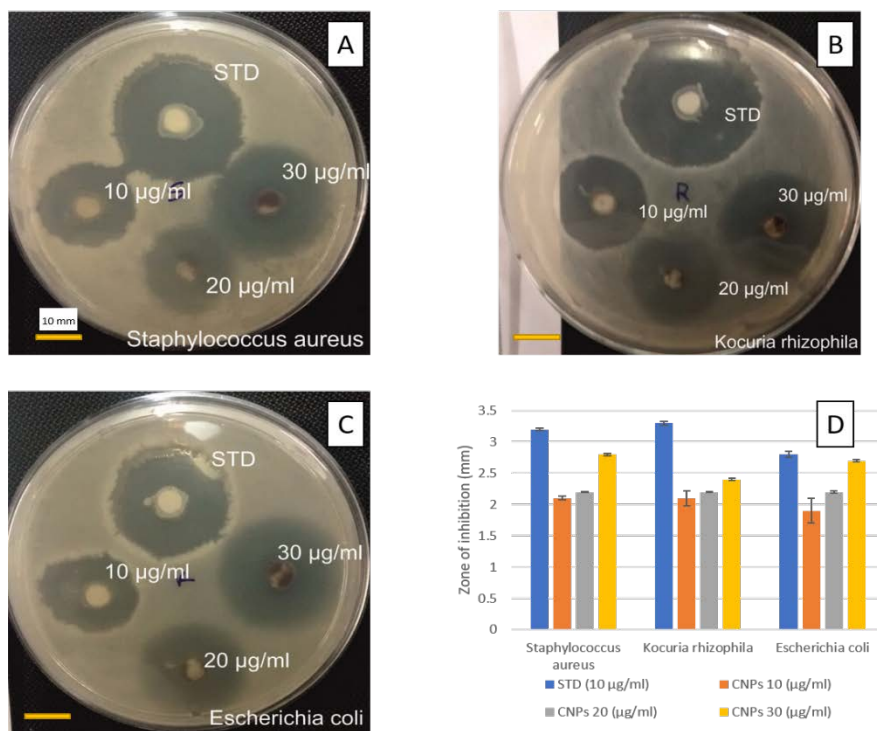


Fig. 3: Kirby-bauer disk diffusion susceptibility studies against (A) *Staphylococcus aureus*, (B) *Kocuria rhizophila*, (C) *Escherichia coli*, to evaluate the zone of inhibition of different concentration of CNPs was compared to STD formulation. (D) shows the zone of inhibition of STD and CNPs (10-30 µg/ml). All values are expressed as, n = 3, mean±SD

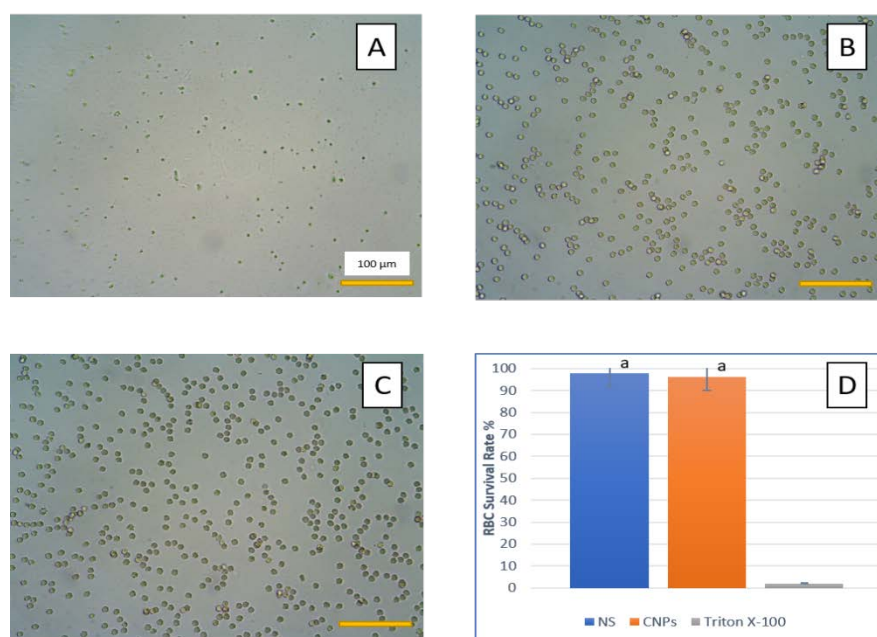


Fig. 4: Biocompatibility studies of CNPs was done by hemocompatibility study (A) shows a microscopic image of STD, (B) NC, (C) CNPs formulation, (D) shows the rate of RBC cell viability of CNPs as compared to normal saline (NS) and, triton X-100. All values are expressed as, n = 6, mean±SD. a =p<0.05 vs positive control

Hemagglutinin assay

Hemagglutinin assay helps to determine the change in morphology of RBCs after exposure to prepared nanoparticles. The blood aggregation was evaluated against untreated RBC in normal saline consisting of biconcave shaped RBCs cells. The CNPs treated RBCs (fig. 4 A, B, and C) showed no significant hemagglutination indicating high biocompatibility [28].

RBC cell viability assay

RBC cell viability assay helps in the determination of biocompatibility of prepared nanoparticles. The CNPs treated RBCs samples were evaluated against the STD suspension of RBC in normal saline solution. Hemolysis assay (fig. 4D) indicated no significant hemolysis, resulting in no significant free hemoglobin in the supernatant solution. The rate of hemolysis was found in an acceptable range of less than 5 % [22].

Wound healing study

Single full-thickness wounds of 15 mm diameter were created on all animals, showing significant variation in the initiation and completion of wound healing study. On 5th and the 13th day of the study indicated important phases of wound healing and were

selected for evaluation of histological sections and biochemical parameters. The percentage of wound closure was measured until full closure was obtained in all animals. The percentage of wound closure was expressed in fig. 5, indicating accelerated wound healing in different groups as compared to the control group.

On the 5th day, the percentage wound contraction of the CNPs group was significantly more as compared to the untreated group (20.18 % and 7.72 % respectively). Similarly, on the 13th day, the wound contraction of the CNPs group was 100 %, indicating full recovery, which is significantly higher as compared to other groups, including NC, vehicle control (VC) and STD group [23].

Histology analysis

Histological assessment in fig. 6, of burn tissue at the end of the study protocol revealed the presence of various proinflammatory cytokines. The tissue of NC, VC, and STD control group shows the presence of exudate, leukocyte infiltration, collagen deposition, and incomplete re-epithelization. Whereas the histogram of treatment group tissue shows comparatively low exudate and collagen deposition. Moreover, the treatment group shows, complete re-epithelization, which confirms the accelerated wound healing potential of treatment [29].

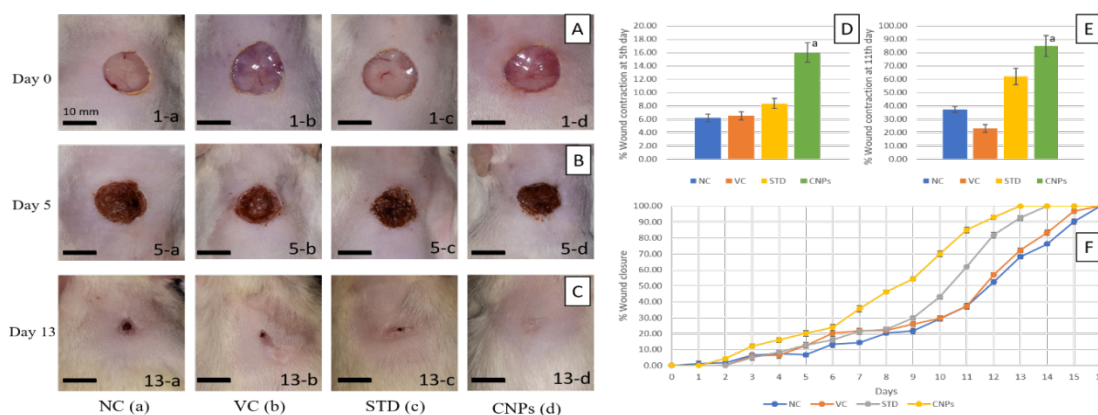


Fig. 5: Healing rate of wound by CNPs was studied, (A) physical observation of wound on day 0, (B) day 5, (C) day 13. (D) shows the percentage wound contraction of the group, NC, VC, STD, and CNPs on day 5th. (E) shows the percentage wound contraction of group, NC, VC, STD, and CNPs on day 11th. (F) shows the percentage wound closure of group NC, VC, STD, and CNPs. All values are expressed as, n = 6, mean±SD. a =p<0.05 vs NC

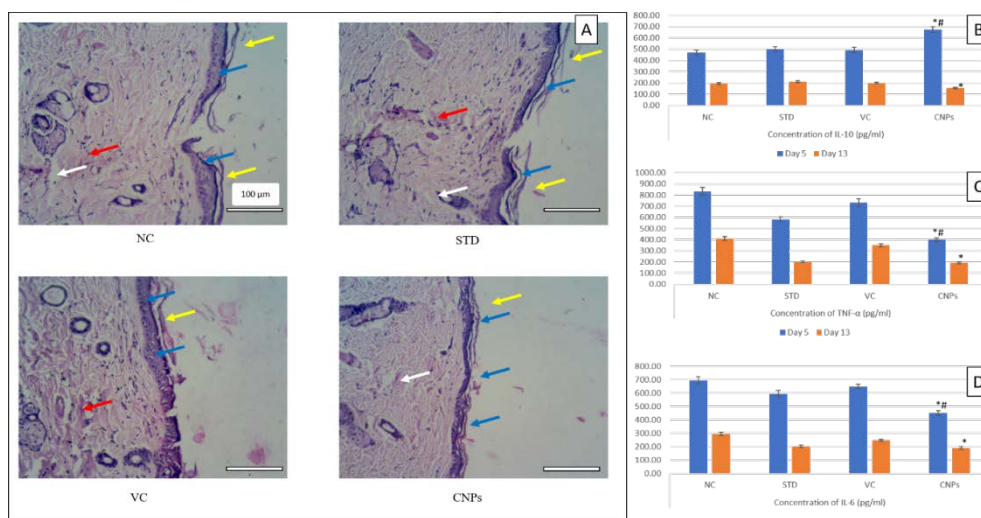


Fig. 6: (A) Histological evaluation at the wound site of different groups (400X) on the 13th day of post-treatment. The presence of leukocyte infiltration, exudate, collagen deposition and re-epithelization was indicated by red, yellow, white and blue arrows, respectively. (B) concentration of IL-10, (C) concentration of TNF-α, (D) concentration of IL-6 on respective groups (NC, STD, VC, CNPs) on the 5th and 13th day. All values are expressed as, n = 6, mean±SD. * =p<0.05 vs. NC, # =p<0.05 vs STD

Inflammatory parameters

Evaluation of pro-inflammatory and anti-inflammatory cytokines supports the result of histological analysis. In fig. 6, the serum IL-6, TNF- α , and IL-10 were done on the 5th and 13th day of study. The evaluation indicated a significantly lower level of pro-inflammatory cytokines (IL-6, 34.6 % and TNF- α , 51.8%) in CNPs formulation treated groups as compared to the NC group [30]. On the other hand, an inversely significant higher concentration of anti-inflammatory cytokines (IL-10, 42.7%) indicated the effectiveness of CNPs for promoting the formation of anti-inflammatory cytokines [31]. A similar trend was obtained on the 13th day, where the concentration of IL-6 and TNF- α was significantly reduced in the CNPs group, as compared to the NC group (35.2% and 53.4 %). Moreover, the concentration of IL-10 was reduced, which indicates faster neutralization of the inflammatory phase by CNPs.

Wound contraction

The wound contraction study on the 5th day indicated significant wound contraction (16.00 %) as compared to NC, while the wound contraction in VC and STD groups was not much significant as compared to NC. On the 13th day, a similar trend was followed. The wound contraction rate of CNPs formulation (85.03 %) was significant as compared to the NC group (37.33 %), which supports the findings of histological analysis, indicating superior wound healing on CNPs (fig. 5). The wound contraction rate study supports the results of the inflammatory cytokines study, indicating the promotion of wound healing and the CNPs helps in acceleration of the wound healing process [32]. The wound diameter was observed on both axes in triplicate to determine the wound contraction rate. The wound contraction rate of CNPs formulation has shown significant contraction, as compared to the NC group and STD group. The rate of contraction of VC was not significant, as compared to no treatment group. The slight faster wound healing in the STD group, as compared to NC and VC group was due to the humectant property of the STD formulation.

DISCUSSION

After induction of wound injury homeostasis, the inflammatory response kicks-in to release cytokines growth factors and chemoattractants to lure lymphocytes and macrophages to the wound site.

Cytokines promote fibroblast migration resulting in endothelial cell proliferation. Fibroblasts release collagen, proteoglycans and glycosaminoglycans, to create the extracellular matrix [33]. The re-epithelization phase is the rate-limiting phase in the wound healing process [29]. The feature of the chronic wound includes a prolongation of the inflammatory phase, with profuse leukocyte infiltration, reduced cellular signaling and fibroblast proliferation.

Attuning pro and anti-inflammatory cytokines is essential for accelerated wound healing. In the present work, we have formulated novel CNPs and evaluated wound healing activity with respect to attuning the inflammatory phases, resulting in the remodeling of excision wound [5]. Our results showed the synthesis of CNPs from copper nitrate solution by the novel cementation method, with particle size in the range of 100-150 nm. The *in vitro* wound healing assay shows faster-wound healing activity significantly as compared to the control group. Further, faster wound healing was observed in the treated groups with topical application of CNPs formulation. CNPs formulation shows best results among all formulations, among all the formulation levels of IL-6, TNF- α levels were observed on 5th and the 11th-day slight increment in levels of IL-10 was observed in case of STD and VC group and significant increment in CNPs group. In CNPs treated group, there is a rapid decrease in levels of pro-inflammatory and anti-inflammatory cytokines, indicating accelerated wound healing, also in CNPs treated group there is a faster deposition of collagens and accelerated re-epithelization was observed. CNPs have also shown to reduce the microbial load and consequently endorse the fast healing of wounds. CNPs show significantly higher wound healing as compared to other groups due to anti-inflammatory activity. Moreover, plausible development of alternatives, this formulation holds strong potential to be explored

for the treatment of chronic non-healing wounds, including burns due to heat, chemical and radiation-induced burn wounds.

CONCLUSION

Consequences of the present investigation conclude that, the formation of copper nanoparticles by the cementation method has a significant purity, with the desirable morphological characteristic of nanoparticles. Copper nanoparticles show significant antibacterial potential, which probably leads to its antimicrobial property that accelerates the wound healing rate. Moreover, the treatment of copper nanoparticles endorses significant wound healing with anti-inflammatory potential, which were confirmed by the assessment of various inflammatory biomarkers. Thus, the study enlightens the therapeutic potential of copper nanoparticles against wound injury by resisting bacterial contamination and significant regulation in inflammatory biomarkers, which may be endorsed as an underlying mechanism.

ACKNOWLEDGMENT

We are highly thankful to the founder president and Amity University for providing lab space and facilitating this research.

FUNDING

This research didn't receive any specific grant from funding agencies in the public, commercial, or non-profit sector.

AUTHORS CONTRIBUTIONS

Ashish Kumar-Formal analysis, writing-original draft, Vinay Pandit-Methodology, investigation, resources, Upendra Nagaich-Writing-review and editing supervision, validation.

CONFLICT OF INTERESTS

The authors declare that they have no competing financial interest or personal relationships that could influence the work reported in the paper.

REFERENCES

- Godbout JP, Glaser R. Stress-induced immune dysregulation: Implications for wound healing, infectious disease and cancer. *J Neuroimmune Pharm* 2006;1:421-7.
- Mühl H. Pro-inflammatory signaling by IL-10 and IL-22: bad habit stirred up by interferons? *Front Immunol* 2013;4:18.
- Chen L, Deng H, Cui H, Fang J, Zuo Z, Deng J, et al. Inflammatory responses and inflammation-associated diseases in organs. *Oncotarget* 2018;9:7204-18.
- Larouche J, Sheoran S, Maruyama K, Martino MM. Immune regulation of skin wound healing: mechanisms and novel therapeutic targets. *Adv Wound Care* 2018;7:209-31.
- Guo S, DiPietro LA. Critical review in oral biology and medicine: factors affecting wound healing. *J Dent Res* 2010;89:219-29.
- Borkow G. Using copper to improve the well-being of the skin. *Curr Chem Biol* 2015;8:89-102.
- Vincent M, Hartemann P, Engels Deutsch M. Antimicrobial applications of copper. *Int J Hyg Environ Health* 2016;219:585-91.
- Mahavir J, Sneh L, Preeti K, Tulika M. Application of nanostructures in antimicrobial therapy. *Int J Appl Pharm* 2018;10:11-25.
- Gopal A, Kant V, Gopalakrishnan A, Tandan SK, Kumar D. Chitosan-based copper nanocomposite accelerates healing in excision wound model in rats. *Eur J Pharmacol* 2014;731:8-19.
- Levy SB, Bonnie M. Antibacterial resistance worldwide: causes, challenges and responses. *Nature Med* 2004;1:122-9.
- Manyasree D, Peddi KM, Ravikumar R. CuO nanoparticles: synthesis, characterization and their bactericidal efficacy. *Int J Appl Pharm* 2017;9:71-4.
- Bahadar H, Maqbool F, Niaz K, Abdollahi M. Toxicity of nanoparticles and an overview of current experimental models. *Iran Biomed J* 2016;20:1-11.
- Sharma AK, Kumar A, Taneja G, Nagaich U, Deep A, Rajput SK. Synthesis and preliminary therapeutic evaluation of copper nanoparticles against diabetes mellitus and-induced micro-(renal) and macro-vascular (vascular endothelial and cardiovascular) abnormalities in rats. *RSC Adv* 2016;6:36870-80.

14. Saber Tehrani M, Rastegar F, Parchehbaf A, Rezvani Z. Determination of copper by flame atomic absorption spectrometry after preconcentration with activated carbon impregnated with a new Schiff base. *Chinese J Chem* 2005;23:1437-42.
15. Chandra S, Kumar A, Tomar PK. Synthesis and characterization of copper nanoparticles by reducing agents. *J Saudi Chem Soc* 2014;1:149-53.
16. Lim J, Yeap SP, Che HX, Low SC. Characterization of the magnetic nanoparticle by dynamic light scattering. *Nanoscale Res Lett* 2013;8:381.
17. Gittings M, Saville D. The determination of hydrodynamic size and zeta potential from electrophoretic mobility and light scattering measurements. *Colloids Surfaces A Physicochem Eng Asp* 1998;141:111-7.
18. Rodriguez P, Plana D, Fermin DJ, Koper MTM. New insights into the catalytic activity of gold nanoparticles for CO oxidation in electrochemical media. *J Catal* 2014;311:182-9.
19. Mühlfeld C, Rothen Rutishauser B, Vanhecke D, Blank F, Gehr P, Ochs M. Visualization and quantitative analysis of nanoparticles in the respiratory tract by transmission electron microscopy. *Part Fibre Toxicol* 2007;4:11.
20. Rades S, Hodoroaba VD, Salge T, Wirth T, Lobera MP, Labrador RH, *et al.* High-resolution imaging with SEM/T-SEM, EDX and SAM as a combined methodical approach for morphological and elemental analyses of single engineered nanoparticles. *RSC Adv* 2014;4:49577-87.
21. Kumar V, Sharma AK, Rajput SK, Pal M, Dhiman N. Pharmacognostic and pharmacological evaluation of *Eulaliopsis binata* plant extracts by measuring *in vitro/in vivo* safety profile and anti-microbial potential. *Toxicol Res* 2018;7:454-64.
22. Shakeel A, Singh A, Das S, Suhag D, Sharma AK, Rajput SK, *et al.* Synthesis and morphological insight of new biocompatible smart hydrogels. *J Polym Res* 2017;24:113.
23. Sangam S, Gupta A, Shakeel A, Bhattacharya R, Sharma AK, Suhag D, *et al.* Sustainable synthesis of single-crystalline sulphur-doped graphene quantum dots for bioimaging and beyond. *Green Chem* 2018;20:4245-59.
24. Mendes JJ, Leandro CI, Bonaparte DP, Pinto AL. A rat model of diabetic wound infection for the evaluation of topical antimicrobial therapies. *Comp Med* 2012;62:37-48.
25. Gal P, Kilik R, Mokry M, Vidinsky B, Vasilenko T, Mozes S, *et al.* Simple method of open skin wound healing model in corticosteroid-treated and diabetic rats: Standardization of semi-quantitative and quantitative histological assessments. *Vet Med* 2008;53:652-9.
26. Kaur P, Sharma AK, Nag D, Das A, Datta S, Ganguli A, *et al.* Novel nano-insulin formulation modulates cytokine secretion and remodeling to accelerate diabetic wound healing. *Nanomed Nanotechnol* 2019;15:47-57.
27. Joseph E, Singhvi G. Multifunctional nanocrystals for cancer therapy: a potential nanocarrier. *Nanomaterials Drug Delivery Ther* 2019;1:91-116.
28. Suhag D, Sharma AK, Patni P, Garg SK, Rajput SK, Chakrabarti S, *et al.* Hydrothermally functionalized biocompatible nitrogen-doped graphene nanosheet based biomimetic platforms for nitric oxide detection. *J Mater Chem B* 2016;4:4780-9.
29. Pastar I, Stojadinovic O, Yin NC, Ramirez H, Nusbaum AG, Sawaya A, *et al.* Epithelialization in wound healing: a comprehensive review. *Adv Wound Care* 2014;3:445-64.
30. Efron PA, Moldawer LL. Cytokines and wound healing: the role of cytokine and anticytokine therapy in the repair response. *J Burn Care Rehabil* 2004;25:149-60.
31. Hussain A, AlAjmi MF, Rehman MT, Amir S, Husain FM, Alsalmeh A, *et al.* Copper(II) complexes as potential anticancer and nonsteroidal anti-inflammatory agents: *in vitro* and *in vivo* studies. *Sci Rep* 2019;9:5237.
32. Bettinger DA, Pellicane JV, Tarry WC, Yager DR, Diegelmann RF, Lee R, *et al.* The role of inflammatory cytokines in wound healing: accelerated healing in endotoxin-resistant mice. *J Trauma* 1994;36:810-3.
33. Strbo N, Yin N, Stojadinovic O. Innate and adaptive immune responses in wound epithelialization. *Adv Wound Care* 2014;3:492-501.